JOURNAL OF CATALYSIS **175,** 16–26 (1998)
ARTICLE NO. CA981975

Mo–V–Nb Oxide Catalysts for the Partial Oxidation of Ethane

I. Preparation and Structural Characterisation

K. Ruth,* R. Kieffer,† and R. Burch*

*Catalysis Research Centre, Department of Chemistry, The University of Reading, Whiteknights, Reading RG6 6AD, England; and †L.E.R.S.I., École Européenne de Chimie Polymères Matériaux de Strasbourg, 1, Rue Blaise Pascal-B.P. 296, 67008 Strasbourg cedex, France
E-mail: scsburch@reading.ac.uk

Received July 21, 1997; revised October 28, 1997; accepted November 4, 1997

A mixed oxide catalyst for the selective oxidation of ethane to ethene and acetic acid, and having the composition Mo(73)V(18) Nb(9)O(x) was prepared and characterised. The crystalline phases found were $Mo_6V_9O_{40}$, $Mo_3Nb_2O_{11}$, and MoO_3; the amorphous part was shown to mainly have the composition Mo(84 ± 3)V(13 ± 3) Nb(2 ± 0.5)O(x). The crystallinity was found to be very sensitive to the calcination temperature in the range 400 to 500°C, where a large part of the amorphous phase is transformed into the crystalline phases given above. The crystalline phases found in the catalyst were prepared separately in pure form, as were additional selected phases from the oxidic system Mo–V–Nb. Analytical transmission electron microscopy was used to determine the contribution of the different phases in the catalyst to the total surface area. It appears that the amorphous phase, shown to consist of small grains (diameter ≈10 nm) and, thus, to have a high surface area, may dominate the properties of the catalyst.

1. INTRODUCTION

Ethane is a cheap, readily available raw material and so the direct catalytic selective oxidation of ethane would be a very attractive route for the production of ethene and acetic acid. For this reason several oxidic catalysts have been tested by various groups for the conversion of ethane to ethene and acetic acid and the main published results are shown in Tables 1 and 2, respectively. While the dehydrogenation process was carried out at atmospheric pressure, for the oxygenation process elevated pressures were applied. These data show that while a large number of catalysts are effective for the dehydrogenation process, only catalysts of the types Mo–V, W–V, V, and V–P were able to catalyse the oxidation process for acetic acid formation. It is noteworthy that these catalysts are also active at low temperatures for the dehydrogenation process. Catalysts of the type Mo–V and W–V showed a higher activity than catalysts of the type V or V–P. For catalysts, composed of oxides of molybdenum, vanadium and niobium the composition effect on the catalytic activity was intensively studied by Thornsteinson *et al.* (1). They found an activity and ethene yield maximum at the composition Mo(73)V(18)Nb(9)O(x) for an unsupported catalyst.

Although there has been a substantial amount of empirical study of mixed oxide catalysts for these reactions, there have been few systematic attempts to relate the structure and composition of the oxide phases to their catalytic properties. The main aim of our work has been to first try to prepare and characterise pure model mixed oxide phases, and then to determine their catalytic properties. In this paper we describe the preparation and structural properties of the catalysts: the catalytic properties are described in the companion paper (2).

2. EXPERIMENTAL

2.1. Catalyst Preparation

The main preparation routes investigated for the preparation of the multiphase catalyst and the binary oxides are summarised in Table 3. The most suitable, regarding crystalline phases and surface area obtained, were selected and are further described below. The preparation of the multiphase catalyst was taken from the literature (3, 4), from which the former was used for further experimental work. For the pure oxides somewhat different methods had to be applied to obtain the necessary oxidation state as well as to ensure the highest possible crystallinity compatible with a sufficient surface area for activity measurements. With the exception of the phases $Mo_3Nb_2O_{11}$ and V_2O_5, all samples were prepared starting with an aqueous solution containing the ions of interest ($(NH_4)_6Mo_7O_{24} \cdot 4H_2O$, NH_4VO_3, and $NbCl_5$). While the ammonium molybdate and vanadate could be used directly, $NbCl_5$ was first decomposed in water and the niobium hydroxide precipitated by neutralisation with NH_4OH solution. After washing of the precipitate

0021-9517/98 $25.00

TABLE 1

Comparison of Oxidic Catalysts Reported in the Literature for the Oxidative Dehydrogenation of Ethane to Ethene at Atmospheric Pressure

Cations in catalyst or oxidic phase	T (°C)	Ethane conversion (%)	Ethene selectivity (%)	Ethene yield (%)	Ref.
Mo, V	390	1	61	0.6	(3)
Mo, V, Nb	390	3	81	2.4	(3)
Mo, V, Nb on Al_2O_3	390	6	62	3.7	(3)
Mo, V, Nb	350	12	89	10.7	(4)
Mo, V, Nb	390	5	89	4.5	(5)
Mo, V, Nb	350	58	65	37.7	(1)
Mo, V, Nb on Al_2O_3	400	50	68	34.0	(1)
Mo, V, Ta on Al_2O_3	400	18	77	13.9	(1)
Mo, V, Sb on Al_2O_3	400	23	75	17.3	(1)
Mo, V, Nb, Sb, Ca[a]	350	34	86	29.2	(6)
Mo, Re, V, Nb, Sb, Ca	325	15	70	10.5	(7)
W, Re, V, Nb, Sb, Li	310	8	80	6.4	(8)
V, P	345	6	77	4.6	(9)
Li, Mg	581	38	80	30.4	(10)
Li, Na,[b] Mg	625	38	85	32.3	(10)
Li, Mg	600	39	75	29.3	(11)
Li, Ti	650	10	92	9.2	(12)
Li, Ti, Mn	650	23	84	19.3	(12)
Sr, Ce, Yb	700	58	70	40.6	(13)
Co, Zr, P, Na, K	675	32	74	23.7	(14)
B, P	550	13	85	11.1	(15)
B_2O_3	550	4	97	3.9	(16)
B_2O_3 on SiO_2	550	4	96	3.8	(16)
B_2O_3 on ZnO	550	35	41	14.4	(16)
B_2O_3 on La_2O_3	550	6	83	5.0	(16)
B_2O_3 on Al_2O_3	550	38	58	22.0	(16)
B_2O_3 on MgO	550	5	80	4.0	(16)
B_2O_3 on P_2O_5	550	2	90	1.8	(16)
B_2O_3 on TiO_2	550	0.4	98	0.4	(16)
B_2O_3 on CaO	550	6	30	1.8	(16)
Sm_2O_3	500	12	54	6.5	(17)
Gd_2O_3	500	12	46	5.5	(17)
V_2O_5	500	6	28	1.7	(18)
V_2O_5 on SiO_2	500	0.14	80	0.1	(18)
V_2O_5	527	8	26	2.1	(19)
V_2O_5 on SiO_2	527	0.5	73	0.4	(19)
V_2O_5 on SiO_2	538	30	22	6.6	(20)
BPO_4	550	0.7	28	0.2	(21)
Na on BPO_4	550	2.4	27	0.6	(21)
La_2O_3	800	73	76	55.5	(22)
CeO_2	800	66	78	51.5	(22)
Sm_2O_3	800	96	28	26.9	(22)
Eu_2O_3	800	79	60	47.4	(22)
Yb_2O_3	800	92	71	65.3	(22)
V_2O_5	500	0.2	50	0.1	(23)
CeO_2	500	44	6	2.6	(23)
Pr_6O_{11}	500	50	21	10.5	(23)
Nd_2O_3	500	48	15	7.2	(23)
$CeVO_4$	500	8	22	1.8	(23)
$PrVO_4$	500	15	5	0.8	(23)
$NdVO_4$	500	15	18	2.7	(23)
VO_2 (B)	343	0.7	80	0.6	(4)
$(VO)_2P_2O_7$	330	25	7	1.8	(24)
$CrPO_4$	550	30	60	18.0	(25)
Cr, ZrP_2O_7	550	24	48	11.5	(25)

[a] Instead of Ca a large number of other promoters were tested and the activity results are given in Ref. (6).

[b] Instead of Na a large number of other elements were tested and the activity results are given in Ref. (10).

with water to remove the chloride it was dissolved again in an aqueous oxalic acid solution. For the preparation of the MoO_3, Nb_2O_5, and the multiphase catalyst the solutions were evaporated at 80°C, and the slurry was dried and calcined. The multiphase catalyst precursor was also calcined at higher temperatures to explore the influence of the calcination temperature on the morphology of the catalyst.

TABLE 2

Comparison of Oxidic Catalysts Reported in the Literature for the Oxidation of Ethane to Acetic Acid

Cations in catalyst or oxidic phase	T (°C)	p (MPa)	Ethane conv. (%)	Ethene sel. (%)	Acetic acid Sel. (%)	Acetic acid Yield (%)	Ref.
Mo, V, Nb	200	0.1	2.3	0	100	2.3	(4)
Mo, V, Nb	325	2	5	66	26	1.3	(1)
W, Re, V, Nb Sb, Li	310	1.4	8	80	9	0.7	(8)
W, Re, V, Nb, Sb, Li	330	2.45	8[c]	47[c]	37[c]	3.0	(8)
W, V, Re, Nb, Sb, Ca	334	1.4	11	53	21[d]	2.3	(7)
W, V, Re, Nb, Sb, Ca	227	2.8	14[c]	12[c]	78[c]	10.9	(7)
VO_2	193	0.1	0.2	0	100	0.2	(4)
V/TiO_2	225	0.1	0.5	8	73	0.4	(26)
V/TiO_2	250	0.1	1	18	36	0.4	(26)
$V, P/TiO_2$	250	0.1	0.5	22	26	0.1	(26)
V, P, Re	335	1.4	4.4	8	27	1.2	(27)

[c] This result was obtained under the presence of water cofeed.

[d] The same measurement with water cofeed led to a selectivity to acetic acid of 49%.

TABLE 3

Preparation Methods Used for the Model Catalysts

Batch composition	Preparation	Colour	XRD	BET
73% Mo 18% V 9% Nb	Mixing of niobium oxalate, NH_4VO_3 and $(NH_4)_6Mo_7O_{24} \cdot 4H_2O$ solutions, evaporation of water during 20 min at 80°C, drying at 120°C, calcination at 400°C for 4 h	Dark green	$Mo_6V_9O_{40}$ $Mo_3Nb_2O_{11}$ MoO_3	10
73% Mo 18% V 9% Nb	Mixing of NH_4VO_3 solution with a suspension of Nb_2O_5 in oxalic acid solution, adding of $(NH_4)_6Mo_7O_{24} \cdot 4H_2O$, drying, grinding, calc. at 250°C for 24 h and at 400°C for 14 h under nitrogen	Black	MoO_2	24
40% Mo 60% V	Calcination of freeze dried precursor at 400°C for 3 h	Dark green	$Mo_6V_9O_{40}$	20
60% Mo 40% Nb	A milled mixture of and MoO_2 and Nb_2O_5, which was previously prepared from a mixture of MoO_3 and metallic Mo, was held at 600°C for 33 h under nitrogen	Bright grey	MoO_2 $Mo_3Nb_2O_{11}$ Nb_2O_5	2
60% Mo 40% V	A milled mixture of MoO_3 and Nb_2O_5 was held at 700°C for 3 h in an evacuated, sealed quartz tube	Bright green	$Mo_3Nb_2O_{11}$	2
50% V 50% Nb	Freeze dried precursor, precalcined at 200°C for 3 h, reduced under hydrogen at 400°C for 3 h and afterwards at 900°C for 3 h	Black	$NbVO_4$	7
50% V 50% Nb	Coprecipitated precursor, precalcined at 200°C for 3 h, reduced under hydrogen at 400°C for 3 h and afterwards at 900°C for 3 h	Black	$NbVO_4$	6

Note. The first preparation method given for each batch composition is the preferred one.

For the preparation of $Mo_6V_9O_{40}$ and $NbVO_4$ the solution was processed by freeze drying. This method avoided a fractional crystallisation of the different components during the concentration of the solution, leading to precursors of high homogeneity. In this process the solutions containing the ions of interest were shock frozen and the pressure then was lowered to 4 Pa for 24 h, holding the temperature at −50°C, to give the precursor which was then calcined. For the formation of $NbVO_4$ the precursor was precalcined at a lower temperature, followed by a heat treatment under hydrogen in two steps at 400 and 900°C. The first step at 400°C was necessary to reduce the volatile V_2O_5 to the high-temperature stable form V_2O_3.

Reaction to the phase $Mo_3Nb_2O_{11}$ was not observed at temperatures lower than 700°C, regardless of the preparation method for the precursor (freeze drying and coprecipitation were tried). Sintering could not be avoided, and for this reason commercial oxides could be used without decreasing the surface area further. To prevent loss of components by volatilisation, the milled mixture of MoO_3 and Nb_2O_5 was sealed in an evacuated silica tube for the heat treatment.

The single oxides MoO_3 and V_2O_5 were formed by calcination of their ammonates at 400°C for 4 h and 550°C for 2 h, respectively. In the case of MoO_3, oxalic acid was added as this doubled the surface area without affecting the crystallinity. Nb_2O_5 was obtained by calcination at 600°C for 2 h of the niobium containing slurry, prepared as described for the multiphase catalyst.

2.2. Catalyst Characterisation

The determination of the crystalline phases in the samples was performed by X-ray powder diffractometry (Siemens D5000 diffractometer), using Cu$K\alpha_1$ radiation. For the determination of the chemical composition of amorphous phases, energy dispersive spectroscopy (EDS) was used in an analytical transmission electron microscope (Phillips CM20, 200 keV). For this purpose, randomly chosen grains were analysed and grouped to give information about the dominant composition of the amorphous phases present. For the observation of the morphology, scanning electron microscopy (SEM) and transmission electron microscopy (TEM) were applied, depending on the purpose (surface or bulk imaging) and the magnification required.

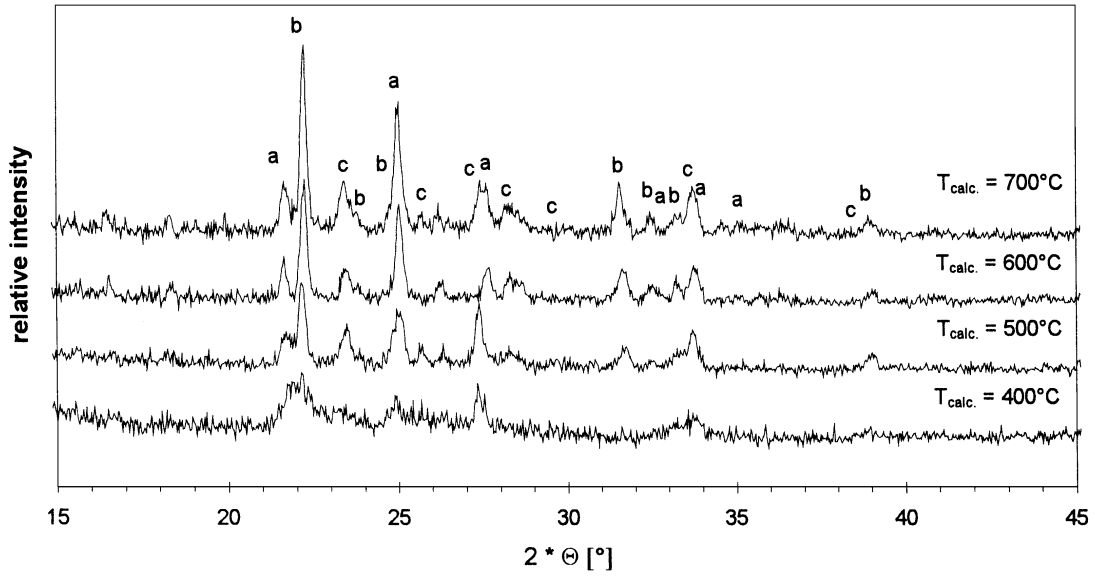

FIG. 1. X-ray powder diffraction pattern of multiphase catalysts, calcined at different temperatures for 4 h, indicating the presence of (a) $Mo_6V_9O_{40}$, (b) $Mo_3Nb_2O_{11}$, and (c) MoO_3 (radiation: $CuK\alpha_1$).

EDS mapping was used to image the elemental distributions in the samples. The possible resolution of these images, consisting of 128×100 points, is limited by the sample thickness, as thicker samples result in greater beam spread and, thus, give a lower spatial resolution in the image. The highest possible resolution finds its limitation in the minimum sample thickness necessary for a signal-to-noise ratio sufficient for the image formation. The resolutions obtained were in the range of 17 nm to 430 nm, depending on the sample thickness. Surface areas were determined by the conventional BET method (nitrogen adsorption).

3. RESULTS

3.1. X-Ray Diffraction Analysis

Multiphase catalyst. Figure 1 shows the X-ray powder diffraction patterns for the multiphase catalyst, calcined at different temperatures. This figure demonstrates that the multiphase catalyst contains the crystalline phases MoO_3 (JCPDS-file 35-609), $Mo_6V_9O_{40}$ (JCPDS-file 34-527), and $Mo_3Nb_2O_{11}$ (JCPDS-file 18-840). However, the formation of these crystalline phases is very temperature dependent. The sample, calcined at 400°C showed only a very weak crystallinity, but the crystalline phases were built up very quickly at higher temperatures. Therefore, the crystallinity for samples calcined at 400°C was difficult to reproduce.

Pure oxide catalysts. All the monophasic catalysts displayed the expected powder diffraction patterns for pure phases (results not reproduced here).

3.2. EDS Analysis of the Multiphase Catalyst

The following compositions have been found by analysing 26 particles[1]:

$Mo(84 \pm 3)$ $V(13 \pm 3)$ $Nb(2 \pm 0.5)$ $O(x)$	(14 particles)
$Mo(55 \pm 4)$ $V(44 \pm 4)$ $Nb(1 \pm 0.4)$ $O(x)$	(4 particles)
$Mo(43 \pm 2)$ $V(57 \pm 2)$ $O(x)$	(6 particles).

The composition of the third type of particles corresponds reasonably closely to the composition of $Mo_6V_9O_{40}$. Although these grains were too small for electron diffraction analysis, it will be assumed that they consist of $Mo_6V_9O_{40}$. It is interesting to note that the composition of each of the first two types of grains are relatively constant again suggesting that they may correspond to single mixed oxide phases although they do not correspond to any reported crystalline phase. In addition, longish crystals of about 100 nm length were found, which contained only molybdenum.

3.3. Surface Area Measurements

The surface areas of the multiphase catalyst and the crystalline phases are given in Table 4. The multiphase catalyst was also calcined at higher temperatures to observe the dependence of the surface area on the treatment temperature. At 500°C the surface area was decreased to below 2 m^2/g. Also, the phase $Mo_6V_9O_{40}$ was calcined at a higher temperature: after calcination at 600°C the surface area was found to have decreased to 1 m^2/g.

[1] The deviations are calculated as standard deviations.

TABLE 4

Surface Areas

Sample	Mo(73)V(18) Nb(9)O(x)	$Mo_6V_9O_{40}$	$Mo_3Nb_2O_{11}$	$NbVO_4$	MoO_3	V_2O_5	Nb_2O_5
Surf. area (m^2/g)	10	20	2	7	4	4	3

3.4. Morphology of the Catalysts

3.4.1. The multiphase catalyst. The multiphase catalyst, calcined at 400°C during preparation, consists of very stable large agglomerates. Its fragments are of irregular shape and have a smooth surface. At a magnification of 500,000 times the individual particles become visible (Fig. 2). The largest fraction has a diameter of only a few nanometers. These were the small grains which were analysed by EDS, leading to the results given in Section 3.2.

An increase in the calcination temperature from 400° to 500°C does not influence the morphology of the aggregates in a significant way, but there is an increase in the number of molybdenum oxide crystallites. On increasing the calcination temperature further to 600°C, some of the crystals had grown to the dimensions of a few micrometers. For these samples, electron diffraction and EDS identified $Mo_6V_9O_{40}$ crystals. Samples calcined at 700°C were shown to be crystalline and contained long MoO_3 needles.

3.4.2. The phase $Mo_6V_9O_{40}$. The secondary electron image of this material (Fig. 3) reveals that the sample $Mo_6V_9O_{40}$ consists of agglomerates of very loose, sponge-like structure. The particles of which this structure is built are of high crystallinity, shown by lattice fringes going through the particles (Fig. 4). A calcination at 600°C led to a dramatic decrease in surface area from 20 m^2/g (when calcined at 400°C) to 1 m^2/g (after calcination at 600°C). This sintering, occurred up to the stage of neck building between the particles with some merging of the particles (Fig. 5). The individual crystal size did not change markedly.

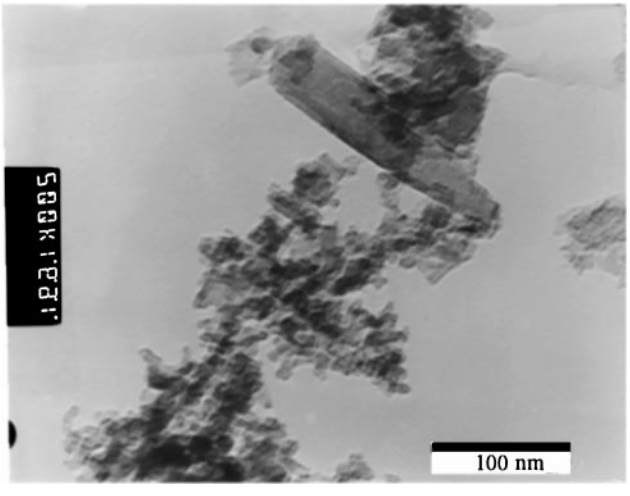

FIG. 2. Multiphase catalyst, calcined at 400°C (bright field image).

3.4.3. The phase $Mo_3Nb_2O_{11}$. The sample of the crystalline structure $Mo_3Nb_2O_{11}$ was a powder with a low surface area of 2 m^2/g and a high powder density. It consists mainly of rectangular shaped crystals with sharp edges. Their side length was about 100 to 200 nm, although some smaller particles were also found.

3.4.4. The phase $NbVO_4$. The sample of the crystalline structure $NbVO_4$ consists of round grains of about 200 nm diameter (Fig. 6).They were partly sintered together, but mainly found as freely moving single particles. The TEM image shows them to have rough, irregular formed surfaces.

3.4.5. The phase MoO_3. The particles in the sample MoO_3 were crystalline with partly rectangular edges, but a large part of the particles had irregular shapes. Particle sizes varied strongly, reaching a maximum of about 500 nm.

3.4.6. The phase V_2O_5. Although rectangular shaped particles were found, most of the particles were of irregular shape and of various sizes in the range up to several hundred nm. Plain surfaces were the most obvious characteristics which these particles had in common.

3.4.7. The phase Nb_2O_5. The Nb_2O_5 crystals had a rectangular, squared shape with plain surfaces and were of about equal size. Their side length was between 100 and 200 nm. They tended to form aggregates.

3.5. Elemental Distribution in the Catalysts

First, the multiphase catalyst was analysed at a low magnification to ensure that large-scale inhomogeneities were not missed during the analysis. The result is given in Fig. 7. Map (a) shows a secondary electron image of the catalyst region analysed. Maps (b), (c), and (d) give the elemental distributions for molybdenum, vanadium, and niobium, respectively. A dark colour corresponds to a high concentration. The spatial resolution of the EDS maps in 430 nm, assuming a maximum sample thickness of 1 μm.

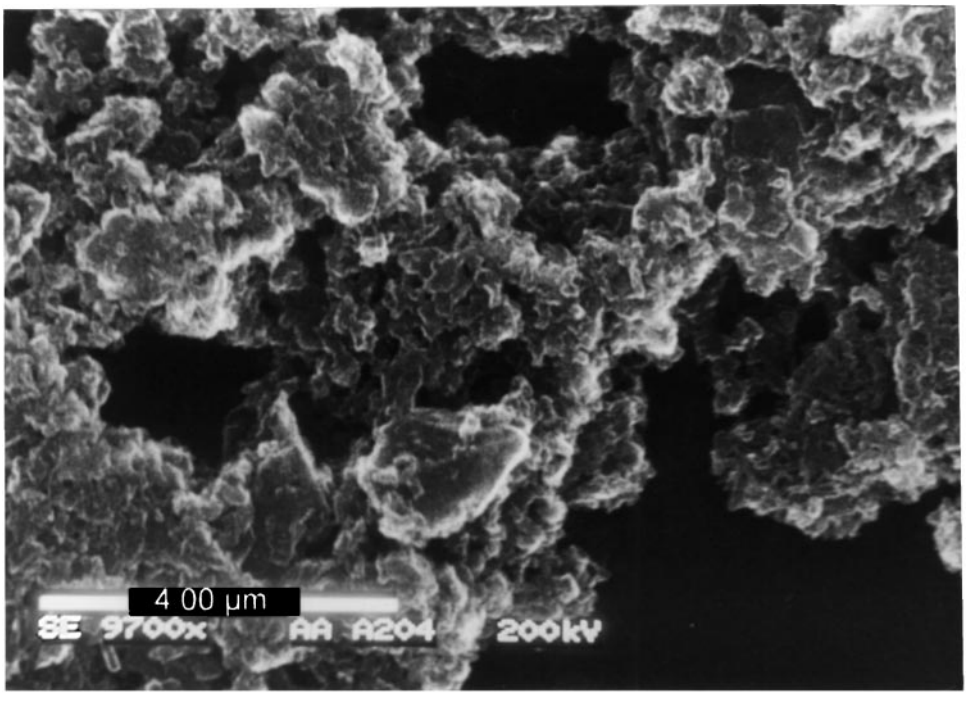

FIG. 3. $Mo_6V_9O_{40}$, calcined at 400°C (secondary electron image).

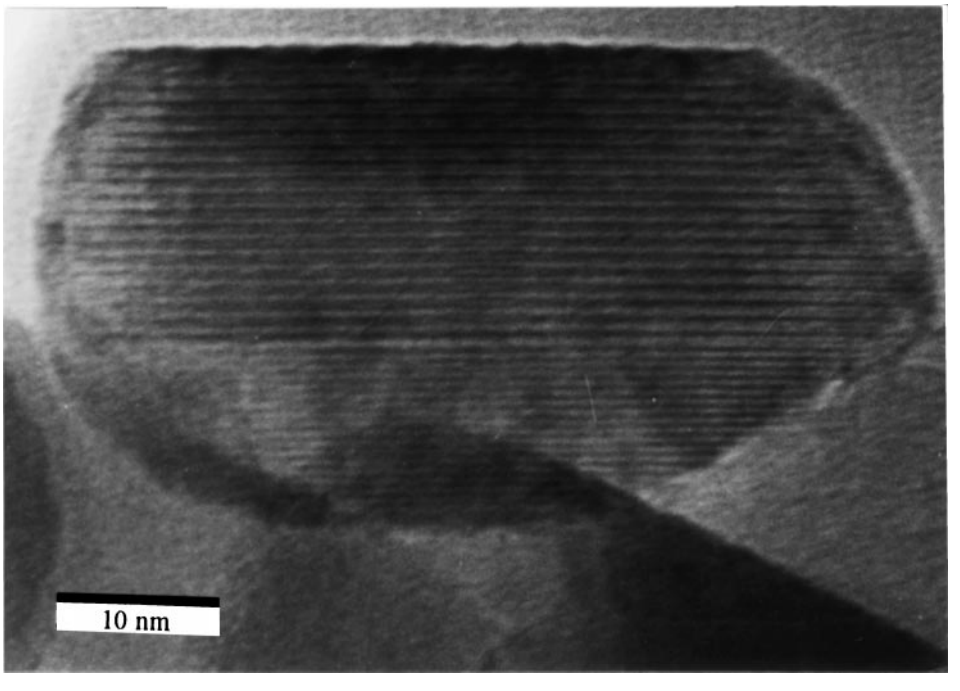

FIG. 4. $Mo_6V_9O_{40}$, calcined at 400°C (bright field image).

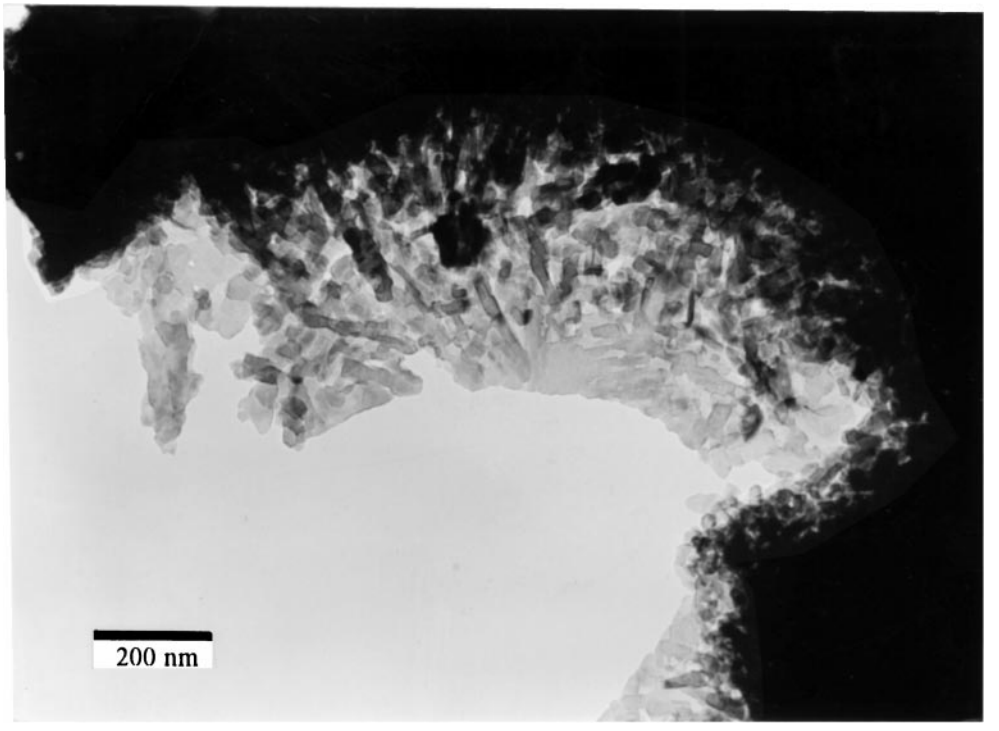

FIG. 5. $Mo_6V_9O_{40}$, calcined at 600°C (bright field image).

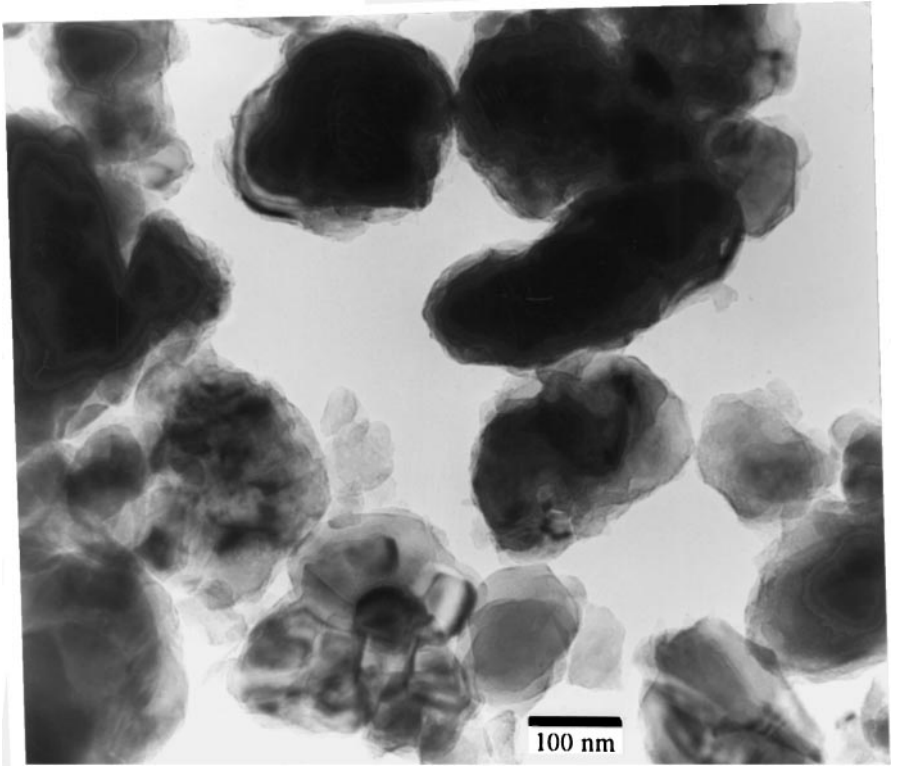

FIG. 6. $NbVO_4$ (bright field image).

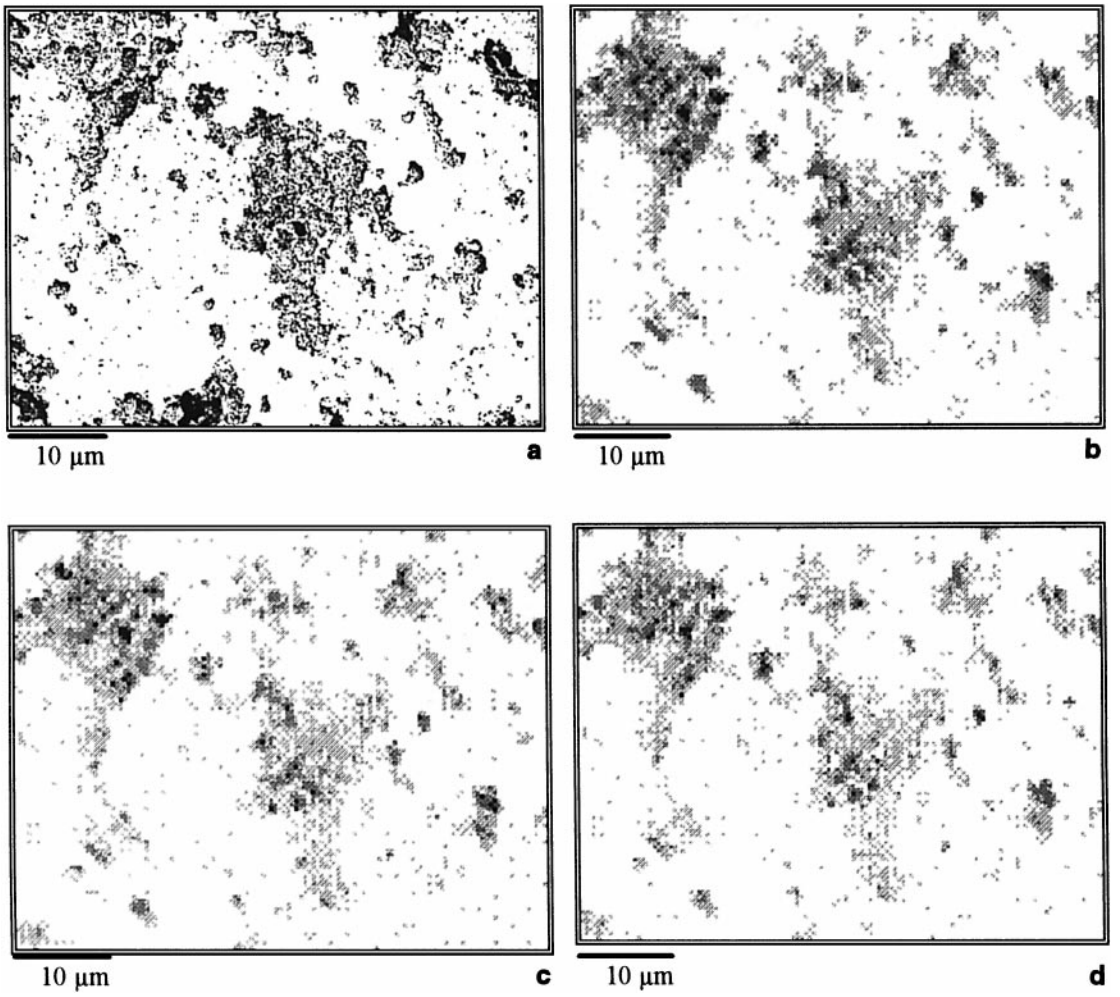

FIG. 7. Multiphase catalyst, calcined at 400°C, elemental distribution measurement by EDS mapping (electron acceleration voltage, 120 kV; counting time per point, 3.4 s). (a) secondary electron image, (b) EDS: molybdenum, (c) EDS: vanadium, (d) EDS: niobium.

Comparison of the EDS maps shows that there are no large-scale elemental composition inhomogeneities; the aggregates are of identical composition within the limits of the quantitative resolution of this type of analysis.

Even when the resolution is increased to below 30 nm EDS-mapping does not show inhomogeneities in the aggregates or significant differences in composition between them. The only inhomogeneities detected were occasional crystals of molybdenum oxide. An example is given in Fig. 8, which shows an EDS map of a part of the sample shown in Fig. 7. While most of the MoO_3 crystals were of round, slightly longish shape, some were found to be needle-like. As the X-ray diffraction measurements showed the presence of $Mo_6V_9O_{40}$ and $Mo_3Nb_2O_{11}$ (Fig. 1), areas containing excess niobium or vanadium should be present. Since these are not detected, we have to assume, therefore, that the dimensions of any structures containing these elements in excess are below the resolution of EDS mapping (i.e., in the case of Fig. 8 smaller than 30 nm).

An EDS map analysis of the multiphase catalyst, calcined at 500°C, is given in Fig. 9. While at most points all three elements were found in reasonable concentration, some particles, most of which were of elongated shape, were of pure molybdenum oxide.

The elemental distributions in the binary oxides were also measured. No significant inhomogeneities were found which might have been missed by XRD-measurements due to a possible low crystallinity.

4. DISCUSSION AND CONCLUSIONS

The X-ray powder diffraction pattern, obtained with the multiphase catalyst, shows that the only crystalline phases present are MoO_3, $Mo_6V_9O_{40}$, and $Mo_3Nb_2O_{11}$. When calcined at 400°C, these were only found in low amounts in the catalyst. However, the largest part of the catalyst consisted of grains containing molybdenum, vanadium and niobium. The EDS-mapping measurements revealed a very

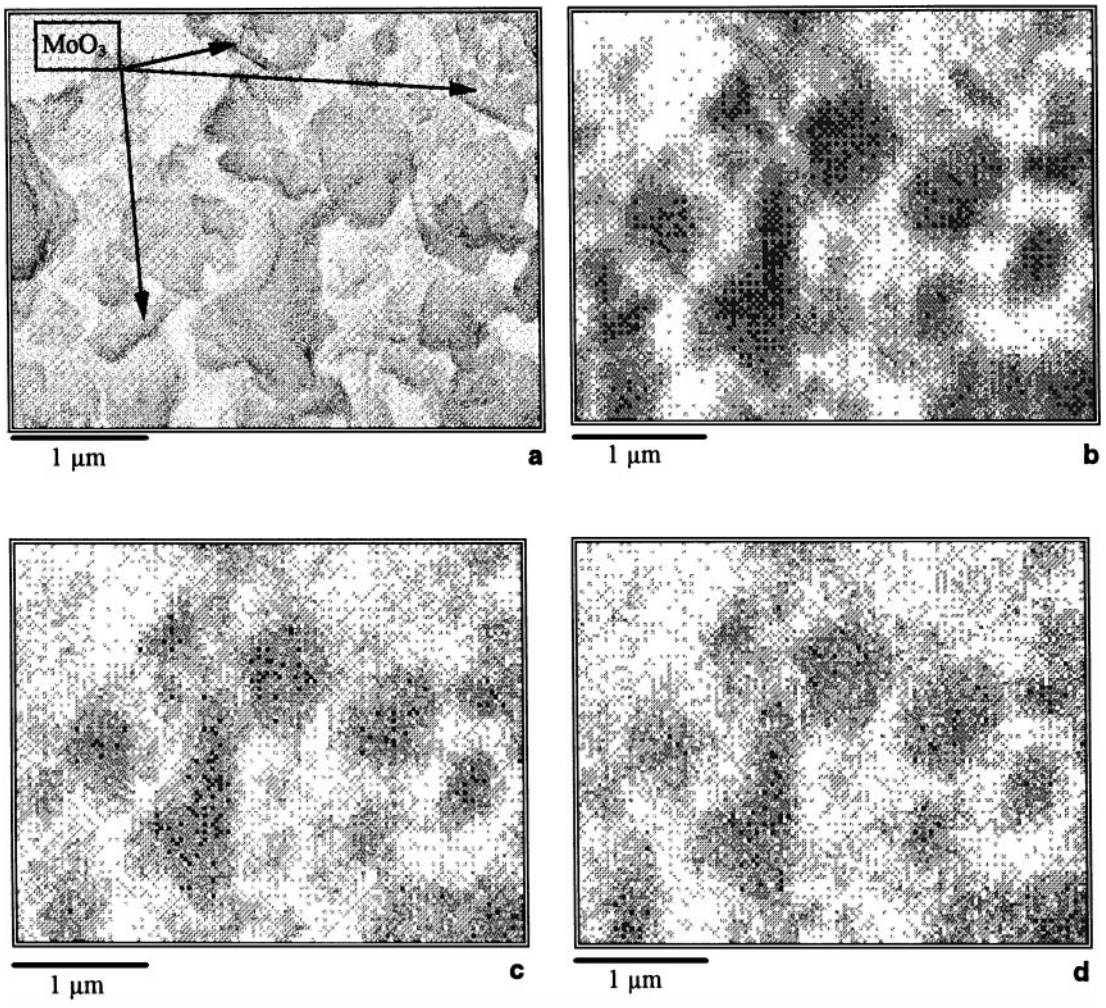

FIG. 8. Multiphase catalyst, calcined at 400°C, elemental distribution measurement by EDS mapping (electron acceleration voltage, 200 kV; counting time per point, 1 s). (a–d) as in Fig. 7.

high degree of homogeneity down to the scale of only about 20 nm.

With increasing calcination temperature the crystalline component of the catalyst increased very quickly at the expense of the amorphous part. In addition, the average size of the particles increases, leading to a lower surface area of the catalyst.

Assuming a complete crystallisation of the sample into the crystalline phases observed, the composition would be (in wt%) 52.2% MoO_3, 25.5% $Mo_6V_9O_{40}$, and 22.3% $Mo_3Nb_2O_{11}$.

The contribution of the different catalytic phases to the total activity of the catalyst is determined by the catalytic properties of the material and by the surface area of each phase rather than by its contribution to the catalyst in weight-percent. As is clear from the electron microscopy and EDS results, the largest fraction of the surface area of the sample calcined at 400°C corresponds to the amorphous grains which have the average composition $Mo(84 \pm 3)V(13 \pm 3)Nb(2 \pm 0.5)O(x)$.

MoO_3 contributes less to the sample surface area than it does to the total sample mass as it comprises large crystals of low surface area. In addition to this phase and the amorphous material, the phases $Mo_6V_9O_{40}$ and $Mo_3Nb_2O_{11}$ have to be considered for their possible contribution to the catalytic activity of the sample. Both appear to have a high surface to mass ratio.

To preserve the amorphous phase, the calcination temperature has to be kept low (e.g., 400°C) to prevent separation into the different crystalline phases. This again makes a careful preparation of the precursor essential in order to allow the formation, at this low temperature, of the amorphous phase, having the composition given above.

The catalytic properties of these catalysts will be described in the companion paper (2).

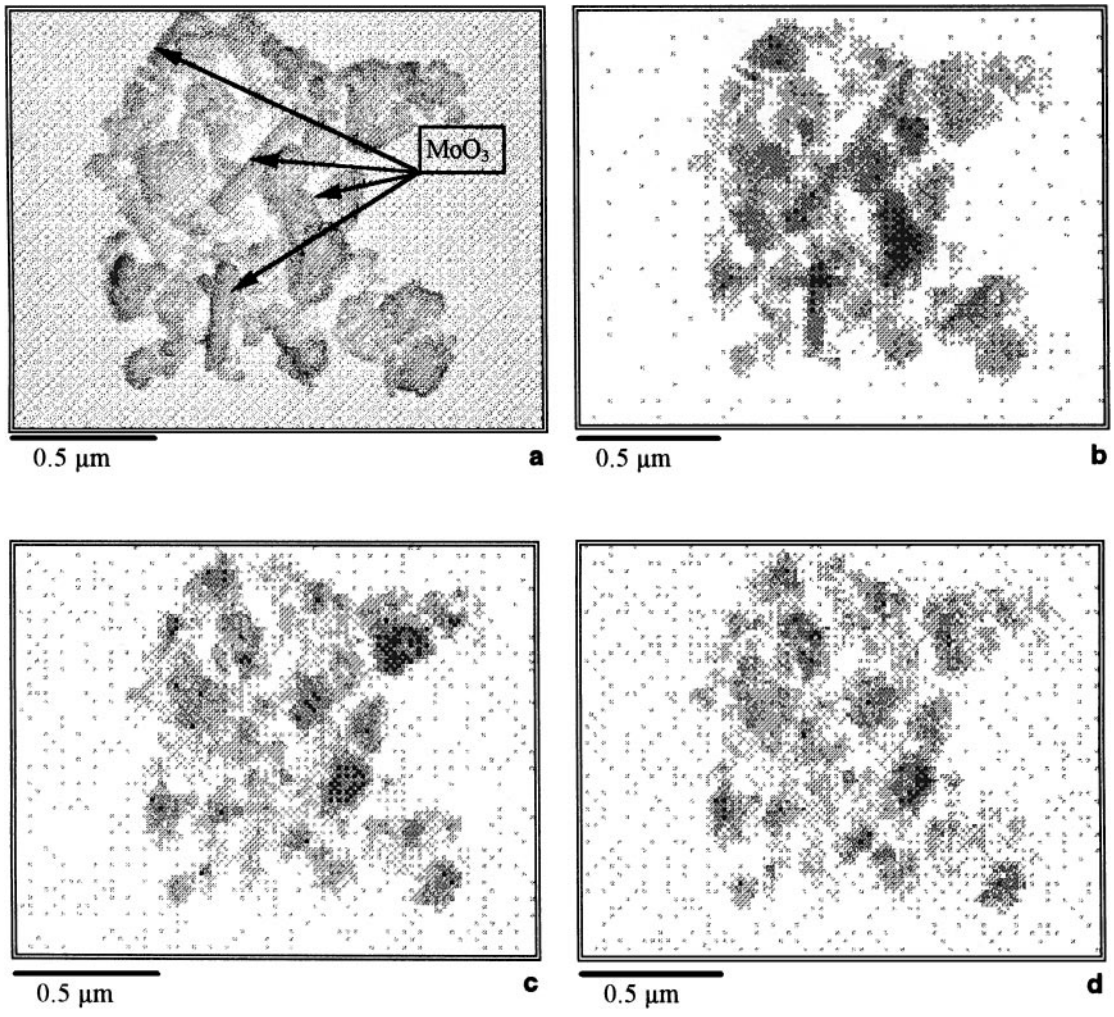

FIG. 9. Multiphase catalyst, calcined at 500°C, elemental distribution measurement by EDS mapping (electron acceleration voltage, 200 kV; counting time per point, 3.4 s). (a–d) as in Fig. 7.

ACKNOWLEDGMENTS

We are pleased to acknowledge financial support from the EU through the Human Capital and Mobility Programme "Catalytic Functionalisation of Lower Hydrocarbons," Contract CHRX CT920065.

REFERENCES

1. Thornsteinson, E. M., Wilson, T. P., Young, F. G., and Kasai, P. H., *J. Catal.* **52**, 116 (1978).
2. Ruth, K., Burch, R., and Kieffer, R., *J. Catal.* **175**, 27 (1998).
3. Burch, R., and Swarnakar, R., *Appl. Catal.* **70**, 129 (1991).
4. Merzouki, M., Taouk, B., Monceaux, L., Bordes, E., and Courtine, P., *in* "New Developments in Selective Oxidation by Heterogeneous Catalysis," p. 165. Elsevier Science, Amsterdam, 1992. [Studies in Surface Science and Catalysis, Vol. 72]
5. Despons, O., Keiski, R. L., and Somorjai, G. A., *Catal. Lett.* **19**, 17 (1993).
6. McCain, J. H., and Charleston, W. V., (Union Carbide), U.S. Patent 4,524,236 (1985).
7. Kitson, M. (BP Chemicals Ltd.), U.S. Patent 5,260,250 (1993).
8. Hallett, C. (BP Chemicals), Europ. Patent 0 480 594 A2 (1991).
9. Michalakos, P., Kung, M. C., Jahan, I., and Kung, H. H., *J. Catal.* **140**, 226 (1993).
10. Swaan, H., Toebes, A., Seshan, K., van Ommen, J. G., and Ross, F. R. H., *Catal. Today* **13**, 629 (1992).
11. Morales, E., and Lunsford, J. H., *J. Catal.* **118**, 255 (1989).
12. Eastman, A. D., and Kimble, J. B., U.S. Patent 4,450,313 (1984).
13. Velle, O. J., Anderson, A., and Jens, K. J., *Catal. Today* **6**, 567 (1990).
14. Eastman, A. D., Guillory, J. P., Cook, C. F., and Kimble J. B., U.S. Patent 4,497,971 (1985).
15. Otsuka, K., Uragami, Y., and Hatano, M., *Catal. Today* **13**, 667 (1992).
16. Murakami, Y., Otsuka, K., Wada, Y., and Morikawa, A., *Bull. Chem. Soc. Jpn.* **63**(2), 340 (1990).
17. Bernal, S., Martin, G. A., Moral, P., and Perrichon, V., *Catal. Lett.* **6**, 231 (1990).
18. Oyama, S. T., *J. Catal.* **128**, 210 (1991).

19. Oyama, S. T., and Somorjai, G. A., *J. Phys. Chem*. **94**, 5022 (1990).
20. Erdöhelyi, A., and Solymosi, F., *J. Catal.* **123**, 31 (1990).
21. Uragami, Y., and Otsuka, K., *J. Chem. Soc. Faraday Trans.* **88**(24), 3605 (1992).
22. Choudhary, V. R., and Rane, V. H., *J. Catal.* **135**, 310 (1992).
23. Castiglioni, J., Kieffer, R., and Poix, P., "Proceedings of the 16th Iberoamerican Symposium on Catalysis, Santiago, Chile, 1994," p. 801.
24. Centi, G., and Trifiro, F., *Catal. Today* **3**, 151 (1988).
25. Han, Y., Zou, Z., Lu, H., and Hui, C., *Shiyou Huagong* **20**(4), 229 (1991) [Chem Abstr. **115** (1992) no. 256685]
26. Tessier, L., Bordes, E., and Gubelmann-Bonneau, M., *Catal. Today* **24**, 335 (1995).
27. Blum, P. R., and Pepera, M. A. (The Standard Oil Corp.), U.S. Patent 5,300,682 (1994).